Covalent bonding and bandgap formation in transition-metal aluminides: di-aluminides of group VIII transition metals

2002 J. Phys.: Condens. Matter 14 5755

(http://iopscience.iop.org/0953-8984/14/23/309)

INSTITUTE OF PHYSICS PUBLISHING JOURNAL OF PHYSICS: CONDENSED MATTER

J. Phys.: Condens. Matter **14** (2002) 5755–5783 PII: S0953-8984(02)36134-4

Covalent bonding and bandgap formation in transition-metal aluminides: di-aluminides of group VIII transition metals

M Krajčí[1,2] **and J Hafner**[1]

[1] Institut für Materialphysik and Center for Computational Materials Science, Universität Wien, Sensengasse 8/12, A-1090 Wien, Austria
[2] Institute of Physics, Slovak Academy of Sciences, Dúbravská cesta 9, SK 84228 Bratislava, Slovakia

E-mail: fyzikraj@savba.sk

Received 23 April 2002
Published 30 May 2002
Online at stacks.iop.org/JPhysCM/14/5755

Abstract

In this paper we study the electronic structure, electron density distribution and bonding mechanism in transition-metal (TM) di-aluminides Al_2TM formed by metals of group VIII (TM = Fe, Ru, Os) and crystal structures of TM di-silicides $C11_b$ ($MoSi_2$), C40 ($CrSi_2$) and C54 ($TiSi_2$). A peculiar feature of the electronic structure of these TM di-aluminides is the existence of a semiconducting gap at the Fermi level. A substitution of a 3d TM by 4d or 5d metal enhances the width of the gap. From the analysis of the charge-density distribution and the crystal-orbital overlap population we conclude that the bonding between atoms has strong covalent character. This is confirmed not only from the enhanced charge density halfway between atoms, but also by a clear bonding–antibonding splitting of the electronic states. Groups of bonding and antibonding states corresponding to a particular bonding configuration of atoms are separated by a gap. As such a gap is observed in all bonding configurations among atoms in the unit cell it results in a gap in the total density of states. The bandgap exists at a certain electron per atom ratio $e/A \approx 4.67$ and also occurs in TM di-aluminides of groups VII and IX. For group VIII TM di-aluminides the Fermi level falls just in the gap.

(Some figures in this article are in colour only in the electronic version)

1. Introduction

Transition-metal (TM) aluminides are known to be of great technological importance and high scientific interest. Al-based compounds of TMs are among the most promising candidates for high-performance structural materials [1]. The reported tensile strength of nanocrystalline

$Al_{94}V_4Fe_2$ is above 1000 MPa, which exceeds the strength of usual technical steels [2]. The physical interest is triggered by the wide variety of physical properties: aluminides form an important class of quasicrystals, with exotic physical and chemical properties [3]. For instance, an icosahedral AlPdRe phase with a stoichiometric composition around $Al_{70.5}Pd_{21}Re_{8.5}$ exhibits anomalously high electrical resistivity. The absolute values of the reported resistivities may be as high as that in doped semiconductors, $\sim$1 Ω cm.

Alloys composed of metallic elements are naturally expected to be metallic too. However, some crystalline TM aluminides, such as $RuAl_2$, were found to be semiconducting. Others such as Al_3V show electronic properties similar to those characteristic for heavy-fermion systems. $FeAl_2$ shows strong spin fluctuations and spin-glass behaviour at low temperatures [4]. Many of these properties have been related to the formation of a hybridization-induced or Kondo (pseudo)gap, but the detailed mechanism of the bandgap formation remains largely unknown.

The anomalous physical properties of TM aluminides are observed mostly in specific crystalline structures. TM di-silicides $TMSi_2$ with the C54 ($TiSi_2$), C40 ($CrSi_2$) or $C11_b$ ($MoSi_2$) structures are one such family of structures. The semiconducting $RuAl_2$ compound belongs to this class. Another example is the B20 (BiF_3) structure [5], in which TM aluminides such as Fe_2VAl exhibit a semiconducting behaviour.

The electronic structures of various TM aluminides have already been theoretically studied by many authors. From recent works we mention a systematic study of the electronic structure and stability of TM aluminides performed by Watson and Weinert [6–8]. They calculated the heat of formation of several tens of 3d and 4d TM aluminides and investigated the relative stability of these phases. In [5] they studied the formation of hybridization-induced bandgaps in TM di-aluminides, particularly in $RuAl_2$ and $FeAl_2$ in the structures of TM di-silicides and of Fe_2VAl in the BiF_3 structure. The electronic structure of $RuAl_2$ and related compounds has also been studied by other authors [9–11]. Springborg and Fischer [11] report the electronic structure of Al_2Ru, Ga_2Ru and Al_2Os in the structure of TM di-silicides.

It appears that the origin of most of the observed anomalies in the TM aluminides is related to the interatomic bonding, which seems to be far from the expected metallic character. Detailed studies of the electronic structure of these systems indicate that in certain specific coordinations of TM atoms covalent bonds between the TM atom and the neighbouring aluminium atoms can be formed. While covalent bonding is quite usual for semiconductors, in metallic compounds such bonds are unusual. A systematic study of the mechanism leading to the formation of covalent bonds in TM aluminides is therefore highly desirable.

Very recently, we have performed a detailed case-study for Al_3V [30]. We could demonstrate that the existence of a very deep pseudogap at the Fermi level is related to the formation of covalent V–Al bonds and to the existence of a characteristic V–Al coordination in the DO_{22} structure favouring the formation of hybrid orbitals.

In this paper we study di-aluminides of group VIII TMs Fe, Ru and Os in the tetragonal $C11_b$, hexagonal C40 and orthorhombic C54 structures. A peculiar and common feature of these structures is the existence of a gap (or a deep pseudogap) in the density of states (DOS) at the Fermi level. The electronic structure of Al_2Fe, Al_2Ru and Al_2Os compounds has been studied using the VASP (Vienna *ab initio* simulation package) program and the TB-LMTO (tight-binding linear-muffin-tin-orbitals) method. We have investigated in detail the electronic structure, charge density distribution and bonding mechanism in the Al_2Fe system. Concerning the most important features of the electronic structure this system can also be considered as a representative one for other TM di-aluminides with 4d and 5d TMs. To demonstrate a structure-induced origin of the bandgap we compare the electronic structure of Al_2Fe with the electronic structure of TMs di-aluminides formed by group VII and IX elements, namely Al_2Mn and Al_2Co. In these systems the bandgap still exists, but its position is shifted above or

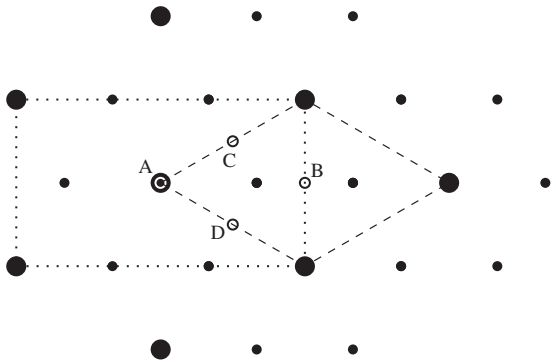

Figure 1. Pseudohexagonal plane common to the C54, C40 and $C11_b$ structures. The four different positions of the central TM in the stacking positions A–D are indicated. The C54 structure contains four layers stacked in the sequence ABCD, the C40 structure contains three layers in ABC stacking and the $C11_b$ structure consists of two layers AB. In the orthorhombic C54 structure the pseudohexagonal layer forms the (001) plane, in the hexagonal C40 structure the (0001) plane and in the tetragonal $C11_b$ structure the (110) plane. The dashed and dotted lines mark the unit cells of C40 and C54 structures.

below the Fermi level. On the basis of the analysis of the charge-density distribution and the crystal-orbital overlap population (COOP) [12] for selected bonding configurations we show that the bonding between pairs of neighbouring atoms in the unit cell has dominantly covalent character. This is confirmed by the enhanced charge density seen halfway between atoms and from the observed bonding–antibonding splitting of the electronic states. In order to better understand the mechanism of bandgap formation we shall also present results for Al_2Fe in the C49 ($ZrSi_2$) crystal structure. This structure slightly differs from the previous family of structures. In the electronic structure of this system there is no bandgap.

Our paper is organized as follows: in section 2 we recapitulate briefly the structural characteristics of the studied system. Section 3 describes the methods used for the calculation of the electronic structures. A picture of the electronic structures of Al_2Fe, Al_2Ru and Al_2Os is presented in section 4.2. A detailed analysis of the charge-density distribution and bonding mechanism in the Al_2Fe system in the $C11_b$, C40, C54 and C49 structures is presented in sections 5–8. Section 9 summarizes our results and evaluates their significance in the current discussion of properties of TM di-aluminides.

2. Crystal structures

We studied the properties of TM di-aluminides in the structure of TM di-silicides, i.e. the C54 ($TiSi_2$), C40 ($CrSi_2$) and $C11_b$ ($MoSi_2$) crystal structures. A unifying feature of these complicated phases is a common structural element, namely nearly hexagonal TM–Al_2 layers [13, 14]. The orthorhombic C54, hexagonal C40 and tetragonal $C11_b$ phases can be generated by changing the stacking sequence of neighbouring TM–Al_2 layers. In particular, the C54 structure contains four layers in an ABCD stacking sequence, the C40 structure contains three layers, ABC, and the $C11_b$ structure consists of two layers with AB stacking. The pseudohexagonal plane and the four different stacking positions A to D are sketched in figure 1. It is remarkable that a similar pseudohexagonal plane also exists in the experimentally determined triclinic structure of Al_2Fe [15]. The second common feature of the considered structures is the same number of nearest neighbours. The Al atom has 14 nearest neighbours;

five of them are TM atoms and nine are Al atoms. Each TM atom has ten Al nearest neighbours and four TM neighbours.

2.1. C54 ($TiSi_2$) crystal structure

The orthorhombic C54 structure, Pearson symbol oF24, belongs to space group $Fddd$ (No 70). The highest point-group symmetry is D_{2h}. There is one Wyckoff position (8a) for TM with two independent positions (0, 0, 0) and ($\frac{1}{4}$, $\frac{1}{4}$, $\frac{1}{4}$), and one position (16e) for Al atoms with four independent positions (u, 0, 0), ($\bar{u}$, 0, 0), ($\frac{1}{4}-u$, $\frac{1}{4}$, $\frac{1}{4}$) and ($\frac{1}{4}+u$, $\frac{1}{4}$, $\frac{1}{4}$). The structure has thus only one internal degree of freedom—the parameter u. An ideal value of this parameter maximizing the packing fraction is $u = 1/3$. The elementary cell consists of 24 atoms; the primitive cell contains six atoms. As already noted above a significant structural feature is the pseudohexagonal plane with TM–Al_2 decoration. This plane is identical here with the (001) plane. Each TM atom has six Al in-plane neighbours arranged on hexagonal vertices centred by a TM atom. Two of the Al atoms lie on the x-axis. There are also two Al neighbours above and two below the hexagonal plane. The latter four Al atoms are arranged around the central TM atom in a somewhat distorted tetrahedral coordination. The additional four TM neighbours also surround the central TM atom in a similar distorted tetrahedral coordination. Each Al site has in the pseudohexagonal plane three Al and three TM neighbours arranged on the vertices of a hexagon centred by the Al atom. There are four additional Al neighbours, two above and two below the (001) plane. These four Al atoms lie in a (011) plane intersecting the (001) plane along the x-axis at the angle of $\alpha \approx 60^\circ$. The remaining two TM neighbours of the Al atom are located above and below the (001) plane in the $(0\bar{1}1)$ plane forming an angle of $-\alpha$ with this plane. Both the (011) and $(0\bar{1}1)$ planes have the same decoration and are related by a pseudo-S_6 symmetry around the x-axis. Note that this symmetry is not related to the pseudohexagonal symmetry in the (001) plane mentioned above. As we shall see in section 7.2, the (001) and (011) planes are important for understanding the chemical bonding in C54-type compounds.

2.2. C40 ($CrSi_2$) crystal structure

The hexagonal C40 structure, Pearson symbol $hP9$, belongs to the space group $P6_222$ (No 180). There is one Wyckoff position (3d) for TM atoms with three independent positions ($\frac{1}{2}$, 0, $\frac{1}{2}$), (0, $\frac{1}{2}$, $\frac{1}{6}$) and ($\frac{1}{2}$, $\frac{1}{2}$, $\frac{5}{6}$) and one position (6j) for Al atoms with six independent sites (u, $2u$, 0.5), ($2\bar{u}$, $\bar{u}$, $\frac{1}{2}$), (u, $\bar{u}$, $\frac{5}{6}$), ($\bar{u}$, $2\bar{u}$, $\frac{1}{2}$), ($2u$, u, $\frac{1}{6}$) and ($\bar{u}$, u, $\frac{5}{6}$). The structure has only one internal degree of freedom—the parameter u. An ideal value of this parameter for densest packing is $u = 1/6$. The (pseudo)hexagonal plane mentioned above is identical here to the (002) plane. The space group is nonsymmorphic, containing nonprimitive translations ($\tau = c/3$ and $2c/3$) which interchange individual hexagonal layers. The decoration of the hexagonal plane by atoms is the same as in the C54 structure. The elementary cell contains nine atoms. The topology of the nearest-neighbour configuration around the TM and Al sites is the same as in the C54 structure.

2.3. $C11_b$ ($MoSi_2$) crystal structure

The tetragonal $C11_b$ structure, Pearson symbol tI6, belongs to the space group $I4/mmm$ (No 139). There is one Wyckoff position (2a) for TM atoms with one independent site (0, 0, 0) and one position (4e) for Al atoms with two independent sites (0, 0, u) and (0, 0, $\bar{u}$). The structure has thus only one internal degree of freedom—the parameter u. An ideal value of

this parameter is $u = 1/3$. The elementary cell contains six atoms, while the primitive cell has three atoms. The pseudohexagonal plane is here identical with the (110) plane. The decoration of the pseudohexagonal plane by atoms is the same as in the C54 structure. The number of nearest neighbours is the same as in the previously discussed structures. The nearest-neighbour environments of TM and Al sites differ from that in the C54 structure in the arrangement of atoms above and below the pseudohexagonal plane. While in the C54 structure the neighbours of Al or TM sites outside the pseudohexagonal plane have tetrahedral arrangement, here all these atoms lie in the $(\bar{1}10)$ plane, perpendicular to the pseudohexagonal (110) plane.

3. Method

3.1. VASP and LMTO

The electronic structure calculations have been performed using two different techniques. The plane-wave-based Vienna *ab initio* simulation package VASP [16, 17] has been used for the calculations of the electronic ground state and for the optimization of the atomic coordinates, volume and geometry of the unit cell for all investigated structures. The theoretical background of VASP is density-functional theory (DFT) within the local-density approximation (LDA). The wavefunctions are expanded in plane waves. The Hamiltonian is based on pseudopotentials derived according to Vanderbilt's recipe [18] for ultrasoft pseudopotentials or projector-augmented-wave (PAW) potentials [17]. VASP performs an iterative diagonalization of the Kohn–Sham Hamiltonian. The plane-wave basis allows us to calculate Hellmann–Feynman forces acting on the atoms and stresses on the unit cell. The total energy may by optimized with respect to the volume and the shape of the unit cell and to the positions of the atoms within the cell. The calculations were performed within the LDA and the generalized-gradient approximation (GGA). For LDA calculations we used the Ceperley–Adler (CA) [19] exchange–correlation functional as parametrized by Perdew and Zunger [20]. For calculations based on the GGA we used the CA parametrization for the LDA part and applied the gradient corrections according to Perdew and Wang [21, 22]. VASP has also been used to calculate charge distributions. In its PAW version [17], VASP calculates the exact all-electron eigenstates, hence it produces electron densities more realistic than those derived from muffin-tin orbitals.

However, a plane-wave-based approach such as used in VASP produces only the Bloch states and the total DOS, a decomposition into local orbitals and local orbital-projected DOSs requiring additional assumptions. To achieve this decomposition, self-consistent electronic structure calculations have been performed using the TB-LMTO method [23–25] in an atomic-sphere approximation (ASA). The minimal LMTO basis includes s, p and d orbitals for each Al and TM atom. The two-centre TB-LMTO Hamiltonian has been constructed and diagonalized using standard diagonalization techniques. The total DOS and band structures produced by both VASP and TB-LMTO techniques are found to be in good agreement. The minimal TB-LMTO basis is then used to construct the symmetrized hybrid orbitals from which the COOPs defined by Hoffmann [12] are calculated.

The COOPs (which are often also referred to as the energy-resolved bond-order, because integrating over occupied states gives the bond-order introduced by Pauling) describe the character and strengths of bonds. This concept has been extended by Dronskowski and Blöchel [26] and Bester and Fähnle [27] to a partitioning of the total energy in the spirit of the tight-binding bond model [28, 29]. However, as our primary aim is to identify the mechanism leading to the formation of a semiconducting bandgap in intermetallic compounds, we shall not quantify the contributions to the bond energies. Bester and Fähnle [27] also point out that the application of the concept of a COOP or of the band-energy partitioning within a

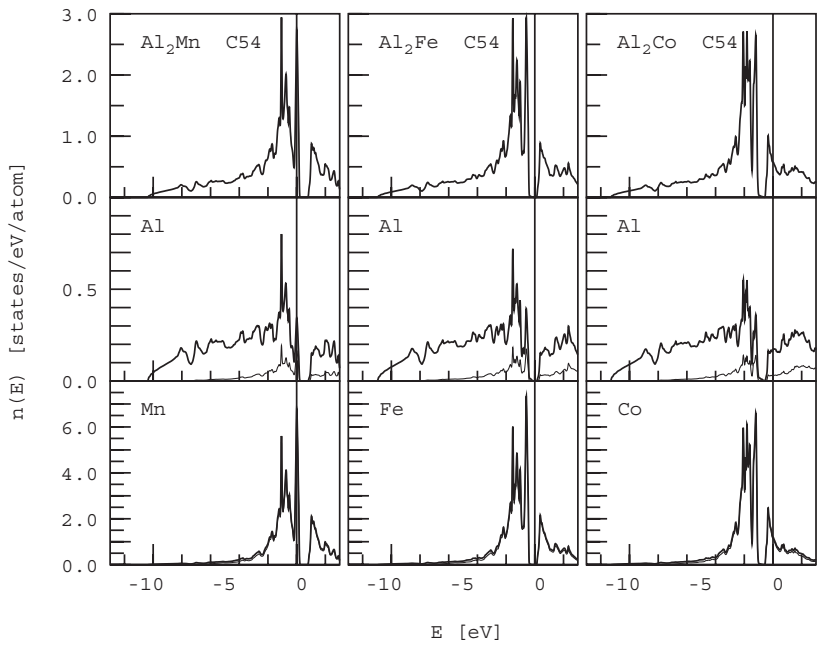

Figure 2. DOS of Al_2TM, TM = Mn, Fe and Co, in the C54 structure: total DOS, partial aluminium DOS and TM DOS. The thin curve represents the contribution from d electrons. Note the bandgap below, at and above the Fermi level for Al_2Mn, Al_2Fe and Al_2Co, respectively.

plane wave or mixed-basis code requires the projection of the Bloch states resulting from the pseudopotential or PAW calculations onto a minimal set of localized orbitals, which implies some arbitrariness in the choice of the localized functions [27]. This arbitrariness is best avoided by performing a TB-LMTO calculation (or any other calculation based on a minimal basis of localized orbitals) 'on top' of the plane-wave optimized structure. Given the efficiency of the TB-LMTO technique, the added computational effort is quite small.

Many of the compounds investigated here possess the same type of lattice and can be considered as isostructural. However, lattice constants and internal coordinates can vary from one compound to another. Hence, for each structural model of each compound the forces and stress tensor have been calculated and the positions of all atoms in the cell and the lattice constants have been optimized. The optimizations are performed for all systems including those for which crystallographic data are available. The structural relaxation has a significant effect on the resulting electronic structure. For instance, the width of the bandgap at the Fermi level for the Al_4MnCo compound in the C54 structure increased from 0.15 eV for a nonrelaxed lattice to 0.51 eV for the fully relaxed one.

4. Electronic density of states of transition-metal di-aluminides

4.1. Al_2TM, $TM = Mn, Fe, Co$

The electronic structure of the TM di-aluminides has been calculated using the VASP and TB-LMTO methods. Figure 2 shows the DOS of Al_2TM compounds in the C54 structure for three third-row TMs (TM = Mn, Fe and Co) calculated using VASP. It presents the total, partial aluminium and TM DOS. The most remarkable feature is a narrow gap ($E_g \approx 0.5$ eV)

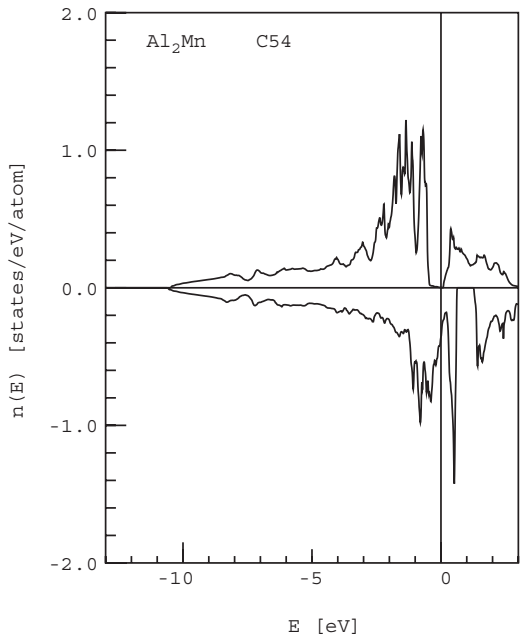

Figure 3. Spin-polarized total DOS of ferromagnetic Al_2Mn in the C54 structure. Note that the Fermi level falls in the bandgap of the majority band, hence ferromagnetic Al_2Mn is half-metallic.

in the band. While for Al_2Mn and Al_2Co the gap is located above and below the Fermi level, respectively, for Al_2Fe the Fermi level falls into the gap. This result demonstrates that the existence of the bandgap is structure induced and for an appropriate electron-per-atom ratio the Fermi level can fall into the gap. Al_2Fe in C54 structure should therefore be a semiconductor. However, the real existence of such a compound in the phase diagram depends on the possible existence of other compounds of the same or similar composition. In the next section we shall study several such candidates.

For Al_2Mn the position of the Fermi level coincides with a sharp peak of the DOS, which indicates a possibility of a magnetic instability. A spin-polarized calculation shows that the compound is a half-metallic ferromagnet with a moment 1.99 μ_B on the Mn atoms. Figure 3 presents the spin-polarized DOS: for the majority band the Fermi level falls in the bandgap; for minority electrons the gap is shifted about 1 eV above E_F.

4.2. Al_2TM, $TM = Fe, Ru, Os$

4.2.1. Al_2TM in the $C11_b$, C40, C54 structures. The bandgap at the Fermi level for the Al_2TM system becomes broader if a 3d TM is replaced by a 4d or 5d TM. Figure 4 presents a study of the total DOS of Al_2TM compounds assuming the three crystal structures $C11_b$, C40 and C54 and TMs from 3d to 5d: TM = Fe, Ru, Os.

The electronic structure of Al_2Ru in the observed C54 structure has been studied repeatedly [5, 9–11]. The work of Springborg and Fischer [11] reports the electronic structure of Al_2Ru, Ga_2Ru and Al_2Os also calculated for the $C11_b$ and C40 structures.

Equilibrium volume, structural parameters and total energy for Al_2Fe for all three structural variants are given in table 1. The GGA calculation predicts the lowest total energy

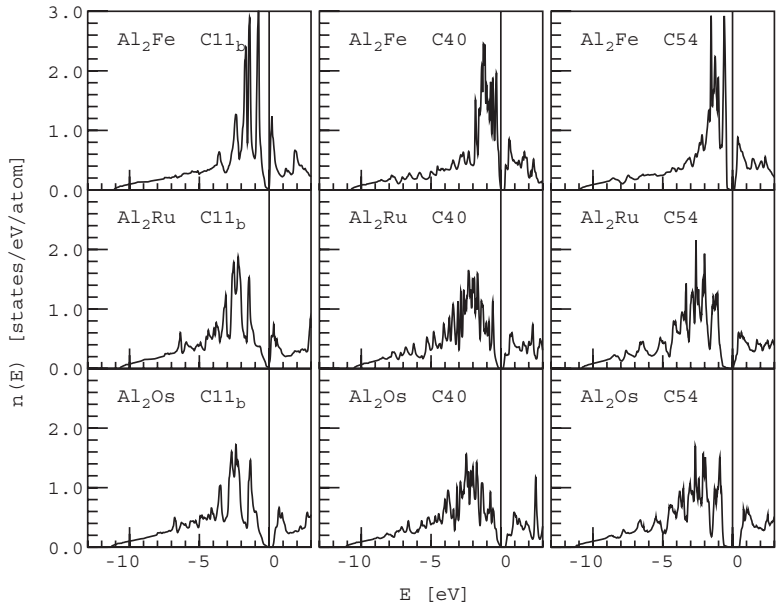

Figure 4. Total DOS of Al_2TM, TM = Fe, Ru, Os, in three crystal structures, $C11_b$ ($MoSi_2$), C_{40} ($CrSi_2$) and C_{54} ($TiSi_2$). The bandgap at the Fermi level widens if Fe is replaced by Ru or Os. It also increases if the crystal structure becomes more complicated—$C11_b$, C_{40} and C_{54} consist of two, three and four pseudohexagonal planes, respectively.

Table 1. Equilibrium lattice parameters a, b/a and c/a, internal coordinate, volume of the cell Ω, total energy E_{tot} and width of the gap at the Fermi level E_g of Al_2Fe for three lattice types.

Al_2Fe	a (Å)	b/a	c/a	u	Ω (Å^3/atom)	E_{tot} (eV/atom)	E_g (eV)
C54 ($TiSi_2$)	7.797	0.594	1.099	0.3256	12.908	−5.5447	0.407/0.147
C40 ($CrSi_2$)	4.562	—	1.415	0.1717	12.931	−5.5301	0.301/0.273
$C11_b$ ($MoSi_2$)	3.003	—	2.834	0.3466	12.798	−5.5654	0.125/0.000

$E_{tot} = -5.5654$ eV/atom for the $C11_b$ structure. This structure corresponds to the AB stacking of the pseudohexagonal planes. The total energies for other two variants corresponding to ABC (C40 structure) and ABCD (C54 structure) stacking are 35 and 21 meV/atom higher. A very remarkable result of the structural relaxation is that the equilibrium volumes of the unit cells are significantly lower than those expected according to Vegard's law. For Al_2Fe in $C11_b$ structure the equilibrium volume is 12.80 Å^3, i.e. substantially lower than the averaged value of 14.53 Å^3 predicted from the equilibrium volumes of fcc Al (16.49 Å^3) and bcc Fe (10.61 Å^3) by Vegard's law. The excess volume is −11.9%. The equilibrium volumes in the C40 and C54 structures are only 1.04 and 0.086% higher, respectively, than that of the $C11_b$ structure.

Table 1 also presents the width of the bandgap for all three phases. The definition of the bandgap in many of these compounds is not easy. The valence-band maximum is found in an isolated band with strong dispersion, hence the sharp drop in the valence-band DOS is followed by a very flat tail extending to higher energies. The paper by Springborg and Fischer [11] suggests that the valence-band maxima occur along Γ–X for $C11_b$, along Γ–A or at the L-point for C40 and at Γ for C54. These maxima really stand out of otherwise rather flat bands. To cope with such a situation, the width of the gap E_g is described by two numbers.

Table 2. Equilibrium lattice parameters a, b/a and c/a, internal coordinate u, volume of the cell Ω, total energy E_{tot} and width of the gap at the Fermi level E_g of Al_2Ru for three lattice types. The last row presents experimental data [32].

Al_2Ru	a (Å)	b/a	c/a	u	Ω (Å^3/atom)	E_{tot} (eV/atom)	E_g (eV)
C54 ($TiSi_2$)	8.071	0.587	1.094	0.3291	14.076	−6.2195	0.387/0.087
C40 ($CrSi_2$)	4.696	—	1.414	0.1698	14.101	−6.2026	0.348/0.174
$C11_b$ ($MoSi_2$)	3.153	—	2.688	0.3405	14.048	−6.1818	0.000/0.000
C54 ($TiSi_2$) exp. data	8.012	0.589	1.096	0.3296	13.834	—	

Table 3. Equilibrium lattice parameters a, b/a and c/a, internal coordinate u, volume of the cell Ω, total energy E_{tot} and width of the gap at the Fermi level E_g of Al_2Os for three lattice types. The last row presents experimental data [32].

Al_2Os	a (Å)	b/a	c/a	u	Ω (Å^3/atom)	E_{tot} (eV/atom)	E_g (eV)
C54 ($TiSi_2$)	8.107	0.581	1.095	0.3308	14.130	−6.7449	0.824/0.483
C40 ($CrSi_2$)	4.690	—	1.425	0.1681	14.156	−6.7314	0.369/0.331
$C11_b$ ($MoSi_2$)	3.184	—	2.622	0.3382	14.108	−6.7383	0.439/0.229
$C11_b$ ($MoSi_2$) exp. data	3.162	—	2.625	0.3420	13.831	—	

The first number gives the width of energy interval where the integrated density of states is equal to the total number of electrons in the system with accuracy better than 0.01 electrons. The second number gives the width of energy interval where the total density of states is zero with a numerical accuracy better than 10^{-4} states/eV atom. For further discussion we shall use the former definition. From the table we see that E_g is largest ($E_g = 0.41$ eV) for the C54 structure and smallest ($E_g = 0.13$ eV) for the $C11_b$ structure.

The same physical quantities (equilibrium volume, structural parameters, total energy and width of the bandgaps) calculated for Al_2Ru and Al_2Os are listed in tables 2 and 3, respectively. The Al_2Ru compound is experimentally observed in the C54 structure. On the other hand, Al_2Os crystallizes in the $C11_b$ structure. Our total-energy calculations predict for both systems the lowest energy for the C54 structure. However, for Al_2Os the observed $C11_b$ structure has a total energy only 6 meV/atom higher.

From the tables we see that the bandgap becomes generally broader if a 3d metal is replaced by a 4d or 5d TM. The gap is particularly large for Al_2Os, where for the C54 structure $E_g = 0.82$ eV. The existence of the bandgap in the structure should have a stabilizing effect on the structure. The fact that the experimentally observed phase for Al_2Os is $C11_b$ with smaller bandgap $E_g = 0.44$ eV and not the C54 structure is presumably related to the volume effect. $C11_b$ has generally somewhat lower volume/atom than the C54 structure. In section 5.3 we shall see that in the $C11_b$ structure direct TM–TM bonds that are absent from the C54 structure have clearly covalent character and significantly contribute to the stability of the structure.

In this section we have seen that a semiconducting gap exists for an electron per atom ratio e/A ≈ 4.67 and becomes even broader if Fe, a third-row TM with eight valence electrons, is substituted by a fourth- or fifth-row TM with the same number of valence electrons. However, the semiconducting gap is very sensitive to any interchange of Al and TM sites. When a single pair of Al and TM atoms changes sites the semiconducting gap disappears. This is explicitly demonstrated for the case of C49 structure in section 8. On the other hand the TM sites may be occupied by two different transition metals TM_1 and TM_2. Provided the e/A ratio remains the same the bandgap is preserved [31].

5. Electronic structure of Al_2Fe in the $C11_b$ structure

Al_2Fe in the $C11_b$ structure has the lowest total energy of all three crystal structures considered. From the viewpoint of the electronic structure the Al_2Fe can be considered as a representative system of all Al_2TM compounds with the $C11_b$ structure reported in section 4.2. In this section we shall investigate this system in more detail.

5.1. Electronic density of states

The total DOS of Al_2Fe in the $C11_b$ structure has already been presented in figure 4. The partial Al DOS is dominated by s and p orbitals, but the contribution from d states is also substantial at energies around the Fermi level. The partial Fe DOS around E_F has almost uniquely d character. The s states on the Fe atom extend far below the Fermi level. They contribute to bonding by forming hybrid orbitals with d states. Figure 5 presents an orbital decomposition of the d DOS on the Fe atom. The exact point-group symmetry of this site is D_{4h}. The assignment of individual d orbitals to irreducible representations with the same transformation properties is the following: A_{1g}, d_{z^2}; B_{1g}, $d_{x^2-y^2}$; B_{2g}, d_{xy}; E_g, (d_{zx}, d_{yz}). Note that as the d_{zx} and d_{yz} orbitals belong to the same irreducible representation, their orbital contributions to the DOS are the same. However, as the neighbouring eight Al atoms around the Fe site have an almost cubic configuration, the analysis of orbital contributions can also be performed in terms of the t_{2g} (d_{xy}, d_{yz}, d_{xz}) and e_g (d_{z^2}, $d_{x^2-y^2}$) representations of the O_h space group. Such analysis shows that t_{2g} and e_g orbitals have quite different character. Whereas for e_g orbitals we find only a very narrow gap, with a sharp onset of empty states just above E_F, the unoccupied t_{2g} states are shifted to very high energies.

In the following we attempt to localize covalent bonds in the structure by analysing the difference electron densities and to determine the hybrid orbitals forming these bonds using a group-theoretical analysis.

5.2. Charge density distribution

Using the VASP program we calculated the charge-density distribution of Al_2Fe in the elementary cell of the $C11_b$ structure. To study a possible covalent bonding we investigated the difference electron density, i.e. a superposition of atomic charge densities is subtracted from the total charge density. Figure 6 shows a contour plot of the difference valence-charge distribution in the (001) plane. The positions of Fe atoms are marked by filled circles. To facilitate the analysis a schematic sketch of the tetragonal unit cell is shown in figure 8, highlighting the environment of the TM atom. The contour plot in figure 6 represents the regions of positive difference electron density in the (001) plane; in the blank space the difference density is negative. If the character of the bonding is purely metallic, the charge distribution among atoms should be homogenous. A possible covalency is indicated by enhanced charge distribution along connections between atoms. In figure 6 we see regions of enhanced charge density halfway between the Fe atoms arranged on the corners of a square (cf figure 8).

The enhancement of the charge density between atoms indicates a certain degree of covalency, but it does not immediately imply that a bond is covalent. We shall consider a bond to be covalent if the COOP analysis (see in the next section) shows that there is a gap between bonding and antibonding states. The enhanced charge density thus indicates only the possibility of formation of a covalent bond.

The pseudohexagonal plane in the $C11_b$ structure is identical with the (110) plane. Because of the tetragonal symmetry this plane is equivalent to $(\bar{1}10)$, perpendicular to the (110) plane

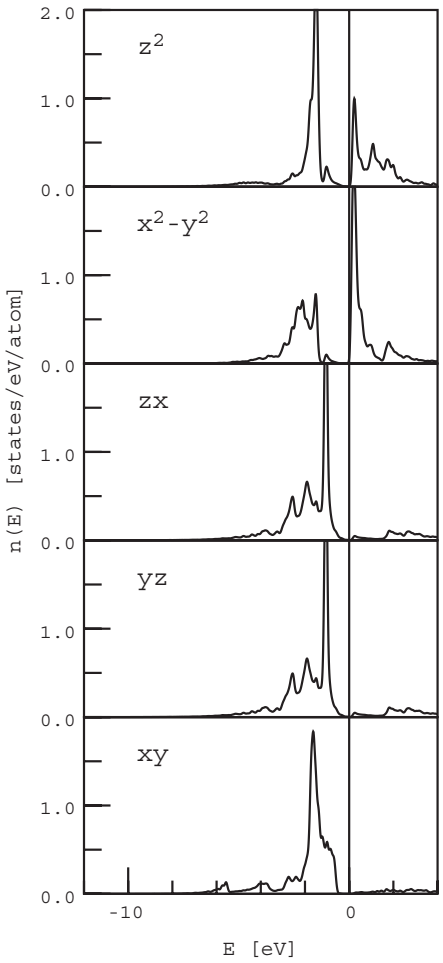

Figure 5. Orbital decomposition of the partial d DOS on the Fe atom in Al_2Fe with the tetragonal $C11_b$ ($MoSi_2$) structure.

(see also figure 8). Figure 7 shows a contour plot of the difference valence-charge distribution in the (110) plane. The positions of Fe atoms are marked by filled circles; positions of Al atoms are marked by open circles. An enhanced charge density is seen along the z-direction between the Fe atom and two Al atoms. There are also enhanced charge densities between Fe and the other four neighbouring Al atoms. Due to the elongated shape of the unit cell the perfect hexagonal symmetry of the charge distribution is broken. The four Al atoms in the (110) plane together with the other four equivalent atoms from the perpendicular $(0\bar{1}1)$ plane form a distorted cubic coordination shell around the central Fe atom.

In summary, there are three types of possibly covalent bond. (i) In the (001) plane iron is bonded to four neighbouring Fe atoms located on the corners of a square. As d orbitals always have inversion symmetry, bonds of Fe with Al atoms occur in pairs of Al atoms in opposite directions. There are two types of bond between Fe and Al atoms. One is directed along the z-axis (ii); four bonds are oriented along body diagonals of the cube (iii). The bonds are marked in figure 8. The character of the bonds is investigated in the next section.

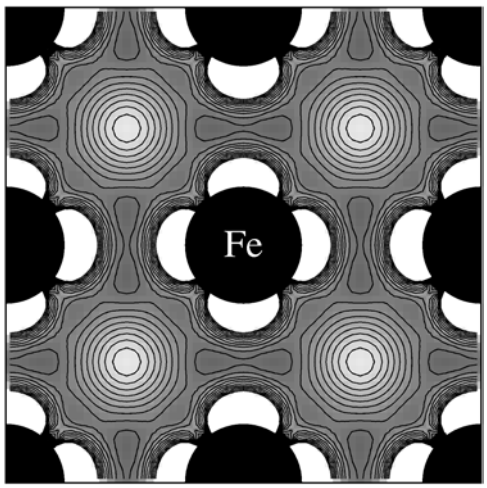

Figure 6. Charge-density distribution in the elementary cell of Al_2Fe with the $C11_b$ structure. The figure shows a contour plot of the difference valence-charge distribution in the (001) plane. The positions of Fe atoms are marked by filled circles. The contour plot represents the regions of positive difference electron density; in the blank space the difference density is negative. A possible covalent bonding is indicated by enhanced charge distribution along connections between atoms. One can see a region of enhanced charge density halfway between each two Fe atoms located in vertices of a square edge.

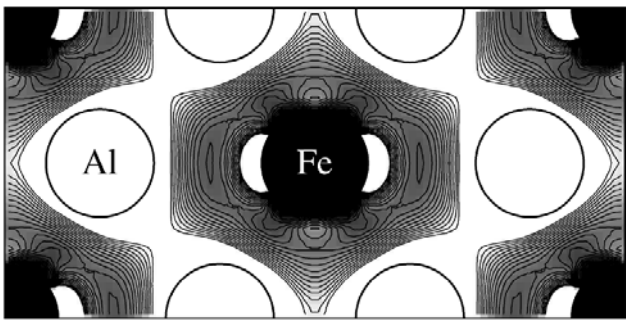

Figure 7. Contour plot of the difference valence-charge distribution of Al_2Fe ($C11_b$) in the pseudohexagonal (110) plane (cf figure 6). An enhanced charge density is seen along the z-direction (horizontal) between the Fe atom and two Al atoms above and below. There are also enhanced charge densities between Fe and four other neighbouring Al atoms. The charge distribution and the elongated shape of the unit cell break the perfect hexagonal symmetry of the plane.

5.3. Hybridized orbitals and covalent bonding

To gain a deeper understanding of the bonds identified in the density contour plots, we attempted to construct sets of symmetrized hybridized orbitals oriented along the bonds and calculated the DOS projected onto bonding and antibonding combinations of these symmetrized orbitals. The difference (B − A) between bonding (B) and antibonding (A) projected densities is essentially equivalent to the differential COOP defined by Hoffmann [12]. Positive values of COOP indicate bonding, negative antibonding character of the states.

The symmetrized orbitals are sets of hybridized orbitals possessing the point-group symmetry of a particular atomic site. A set of bonds originating from a particular atom forms

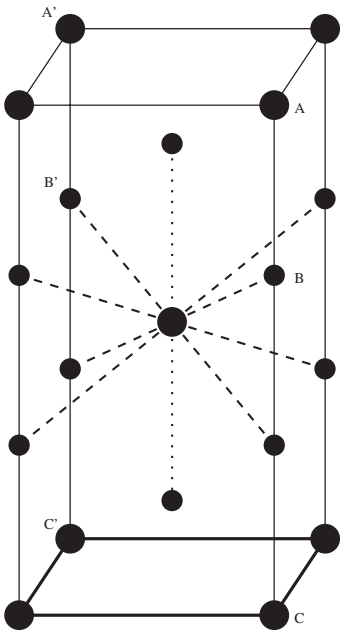

Figure 8. Tetragonal unit cell of the $C11_b$ structure. Large circles—TM atoms, smaller circles—Al atoms. The two different types of Fe–Al bond are marked by dashed and dotted lines, respectively. The Fe–Fe bonds are marked by thicker full lines. The C49 structure can be obtained from the $C11_b$ structure by interchanging the occupation of pairs of atoms A, B and A′, B′. As C = A and C′ = A′, sites C and C′ will also have Al occupation.

a reducible representation of the point group. Decomposition of the reducible representation into irreducible ones enables us to select individual s, p or d orbitals whose linear combinations form symmetrized hybrid orbitals.

Similarly as in our recent study of bonding in Al_3V in the DO_{22} structure [30], the symmetry of $C11_b$ is tetragonal. The point-group symmetry of the iron site is D_{4h}. The orbitals directed from the central Fe atom to the eight Al atoms at the vertices of a tetragonal prism (almost a cube) and to the two other Al atoms located along z-axis form the basis of a reducible representation of the D_{4h} point group. Reduction yields four one-dimensional representations, A_{1g}, A_{2u}, B_{1u} and B_{2g}, and two two-dimensional representations, E_g and E_u. The assignment of atomic orbitals to the irreducible representations with the same transformation properties is the following: A_{1g}, s or d_{z^2}; A_{2u}, p_z; B_{1u}, f_{xyz}; B_{2g}, d_{xy}; E_g, (d_{zx}, d_{yz}); E_u, (p_x, p_y); leading to sp^3d^3f or p^3d^4f hybrid orbitals on the iron atom. The contribution of p states to the iron DOS is small. The same holds also for f states. Therefore sd^3 hybrid orbitals formed by s, $d_{x^2-y^2}$, d_{zx} and d_{yz} states (or d^4 hybridization if we consider the d_{z^2} orbital instead of s) dominate the bonding. The d_{z^2} orbital apparently participates in bonding Fe to two Al atoms located along the z-axis. It is remarkable that the symmetry here excludes the $d_{x^2-y^2}$ orbital from bonding. This is in turn the orbital which plays the dominant role in the Fe–Fe bonding in the tetragonal (001) plane.

It is also important to emphasize that mostly orbitals with even orbital quantum number l, d ($l = 2$) or s ($l = 0$), contribute to the hybridized orbitals on the Fe atom, which therefore have inversion symmetry. Skipping p and f orbitals from the sp^3d^3f hybrids we obtain instead of eight symmetrized orbitals pointing towards the vertices of a tetragonal prism four sd^3 (or d^4) hybridized orbitals possessing inversion symmetry. The symmetrized sd^3 orbitals have a

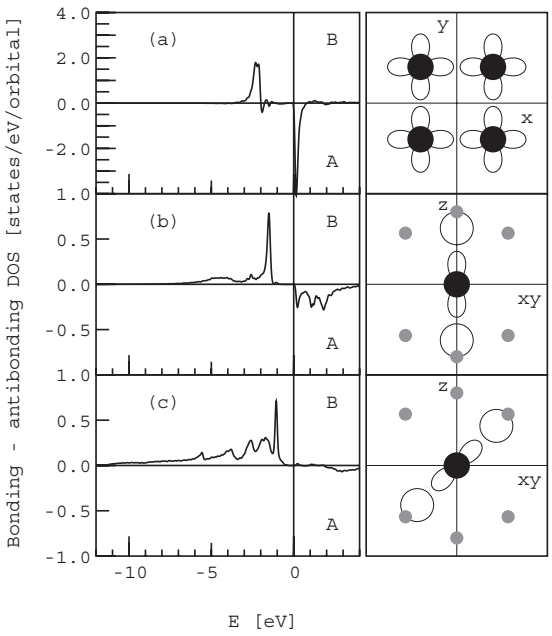

Figure 9. Differential COOP for Al_2Fe ($C11_b$): (a) bonding between Fe $d_{x^2-y^2}$ orbitals in the tetragonal (001) plane, (b) bonding of an Fe d_{z^2} orbital with two sp hybridized orbitals on Al atoms and (c) bonding of a sd^3 hybridized orbital on the Fe atom with sp^3d hybridized orbitals on Al atoms. In the right panel the configurations of bonding orbitals are schematically displayed. Larger filled circles represent Fe, smaller grey circles Al atoms. The corresponding COOP is presented in the left panels. Positive values indicate bonding (B), negative antibonding (A) character. For each bonding configuration we see a clear bonding–antibonding splitting of states. States below E_F have bonding character, states above E_F have antibonding character. Note that groups of bonding and antibonding states are separated by a gap.

form similar to the d_{z^2} orbital and differ only in orientation. While the d_{z^2} orbital is oriented along the z axis, the symmetrized sd^3 orbitals are oriented along the body diagonals of the tetragonal prism.

Figure 9 shows the differential COOP for

(a) bonding of Fe $d_{x^2-y^2}$ orbitals in the tetragonal (001) plane,
(b) bonding of Fe d_{z^2} orbitals with two sp-hybridized orbitals on Al atoms and
(c) bonding of an sd^3 hybridized orbital on an Fe atom with sp^3d hybridized orbitals on Al atoms.

In the right panel the configurations of bonding orbitals are schematically displayed. The corresponding COOP is presented in the left panels; for each bonding configuration we see a clear bonding–antibonding splitting of states. The COOP changes polarity at the Fermi level: states below E_F have bonding character; states above E_F have antibonding character. Moreover, groups of bonding and antibonding states are separated by a small gap.

Hence we are led to the following conclusions.

(i) The results for the COOP prove that in Al_2Fe in the $C11_b$ structure covalent bonds between Al and Fe atoms and also partially between Fe and Fe atoms are formed. There is no significant bonding between Al atoms.
(ii) The (pseudo)gap in the electronic band arises from bonding–antibonding splitting of the electronic states caused by the covalent bonding.

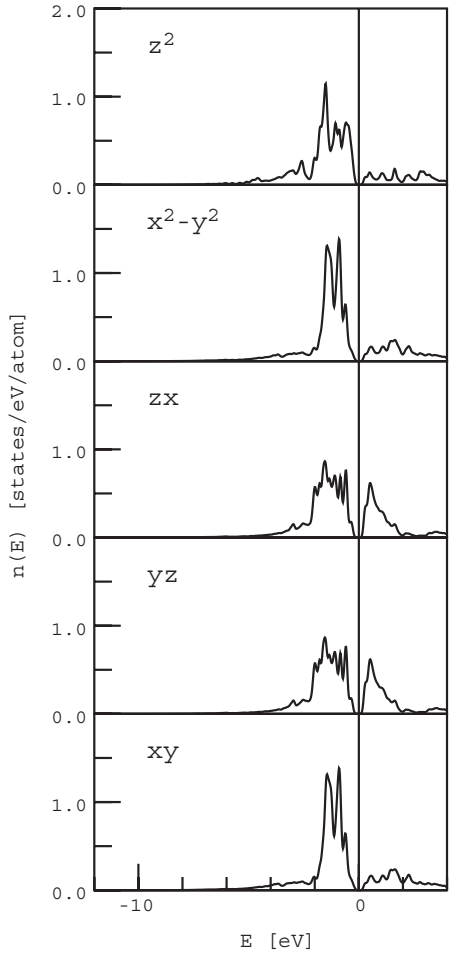

Figure 10. Orbital decomposition of the d DOS on the Fe atom in Al_2Fe in the hexagonal C40 ($CrSi_2$) structure.

6. Electronic structure of Al_2Fe in the C40 structure

The total DOS of Al_2Fe in the C40 structure is seen in figure 4. Figure 10 presents an orbital decomposition of the d DOS on the Fe atom. The highest point-group symmetry of the C40 structure is D_6. The assignment of individual d orbitals to the irreducible representations of the point group D_6 is the following: A_1, d_{z^2}; E_1, (d_{zx}, d_{yz}); E_2, ($d_{x^2-y^2}$, d_{xy}). The orbitals which belong to the same irreducible representation have the same contribution to the DOS. While in-plane bonding of the Fe atom with neighbouring Al atoms is mediated mostly by the E_2 orbitals d_{xy} and $d_{x^2-y^2}$ orbitals, interplanar bonding is dominated by A_1 and E_1 orbitals.

All d-orbital contributions in figure 4 exhibit clear splitting of the band. Groups of states are separated by a narrow gap at the Fermi level. It is notable that the prevailing part of states corresponding to the A_1 and E_2 orbitals is below the Fermi level while in the case of E_1 orbitals a significant concentration of states is also seen above the Fermi level and therefore cannot contribute to the bonding.

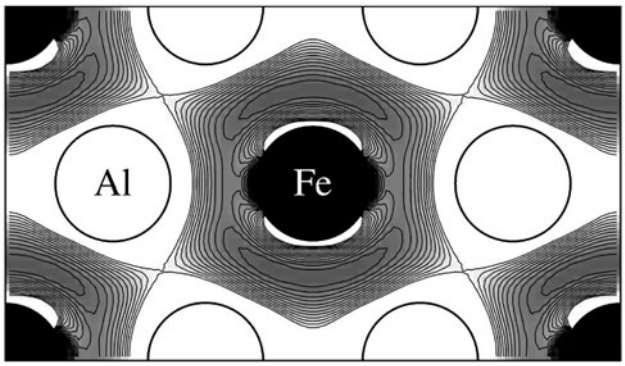

Figure 11. Charge-density distribution of Al_2Fe in the elementary cell of the C40 structure. The results are presented in an orthorhombic supercell. The figure shows a contour plot of the difference valence-charge distribution in the (001) plane. The position of Fe atoms are marked by filled circles, position of Al atoms is marked by open circles. The contour plot represents regions of positive difference electron density; in the blank space the difference density is negative. A possible covalent bonding is indicated by enhanced charge distribution along connections between atoms. One can see a region of enhanced charge density halfway between the central Fe atom and Al neighbours.

6.1. Charge density distribution

Using the VASP program we calculated the charge-density distribution of Al_2Fe in the elementary cell of the C40 structure. To study a possible covalent bonding we investigated the difference electron density. To simplify comparison of the results obtained for the hexagonal C40 structure to other structures we present the C40 results in an orthorhombic supercell. Figure 11 shows a contour plot of the difference valence-charge distribution in the pseudohexagonal (001) plane. The positions of Fe atoms are marked by filled circles, positions of Al atoms are marked by open circles. The contour plot in figure 11 represents the regions of positive difference electron density in the (001) plane, in the blank space the difference density is negative. Although the hexagonal arrangement of atoms in this plane is obvious, the charge distribution a reveals reduction of the D_6 symmetry of the Fe site to D_2. The difference-charge distribution around the Fe atom shows a weak bonding with two Al atoms along the x-direction, but rather strong bonding with the other four neighbouring Al atoms in the pseudohexagonal plane. Compared with the $C11_b$ structure the difference electron distribution around the Fe atom is more evenly distributed.

The Fe atom has ten aluminium neighbours; the remaining four neighbours can be found in the (310) and ($\bar{3}$10) planes. Figure 12 shows a contour plot of the difference valence-charge distribution in the (310) plane. One can easily recognize a strongly enhanced charge distribution below and above each Al atom. The figure reveals that the interplanar bonding between Fe and Al atoms is not co-axial. The strongest charge enhancement is seen approximately near the centre of a triangle formed by one Fe atom and two Al atoms. The bonding charge seen below the Al atoms near the bottom of the figure is a cross-section of enhanced charge in a similar triangle of Fe and two Al atoms in the ($\bar{3}$10) plane. A better understanding of this bonding is given in the next section.

6.2. Hybridized orbitals and covalent bonding

The C40 structure has only one inequivalent Al and one Fe atom, which simplifies the picture of the bonding. The configuration of the Al orbitals participating in the bonding is quite simple. As each Al atom has in the pseudohexagonal (001) plane three Fe neighbours located at the

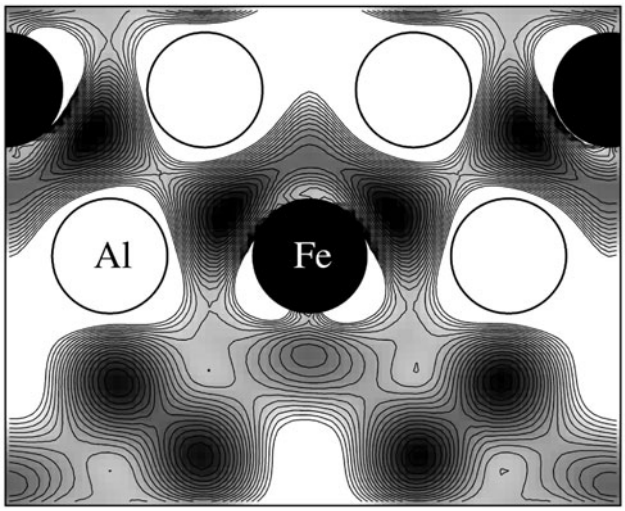

Figure 12. Contour plot of the difference valence-charge distribution in Al_2Fe (C40) in the (310) plane (cf figure 11). The vertical direction corresponds here to the z-axis. One can recognize a strongly enhanced charge distribution below and above each Al atom. The interplanar bonding between Fe and Al atoms is not co-axial. The strongest charge enhancement is seen approximately in the middle of a triangle formed by an Fe atom and two Al atoms. A bonding charge seen below the Al atoms near the bottom of the figure is a cross-section of enhanced charge in a similar triangle of Fe and two Al atoms in $(\bar{3}10)$ plane.

vertices of a triangle, the symmetrized orbitals correspond to sp^2 hybridization, i.e. to a linear combination of s, p_x and p_y orbitals. The remaining p_z orbital participates in bonding between neighbouring pseudohexagonal planes.

Participation of Fe d orbitals in the bonding is more complex. Let us consider first bonding in the pseudohexagonal (001) plane, identical with the (x, y) plane. Figure 13 shows the COOP of several bonding configurations of individual d orbitals on the Fe atom with sp^2 hybrid orbitals on Al: part (a) shows the contribution of the d_{xy} orbital, (b) that of the $d_{x^2-y^2}$ orbital and (c) that of the d_{z^2} orbital to the bonding. In the right panel the configurations of bonding orbitals are schematically displayed; the corresponding COOP is presented in the left panels. For each orbital we see clear bonding–antibonding splitting of states. The COOP changes sign at the Fermi level: states below E_F have bonding character; states above the E_F have antibonding character. We note that even the d_{z^2} orbital makes a significant bonding contribution in the (x, y) plane despite its major orientation in the perpendicular direction. This indicates that each d orbital can non-negligibly participate in every bond. From the set of d orbitals we can also construct hybridized orbitals with a special orientation. Figure 14(a) shows the COOP of d^3 hybrid orbitals which incorporate $d_{x^2-y^2}$, d_{xy} and d_{z^2} orbitals with sp^2 hybrid orbitals of Al in the (x, y) plane. Again we see clear bonding–antibonding splitting of the states. We would also obtain a similar picture for the sd^2 hybrid orbital with s instead of the d_{z^2} orbital.

Interplanar bonding in the C40 structure is more complicated. As one can conclude from the charge distribution analysis the bonding of Fe to Al atoms is not co-axial. Here we analyse the bonding configurations corresponding to the strong charge enhancement in the (310) plane shown in figure 12. From the Al side the p_z orbital oriented along the z-axis and from the Fe side a d^4 hybrid orbital oriented towards the Al atom that includes d_{xy}, d_{yz}, d_{zx} and d_{z^2} orbitals contribute to the bonding. The same d orbitals participate in in-plane and interplanar bonding as well. This also holds for the s orbital. In contrast to the $C11_b$ structure, symmetry here does not

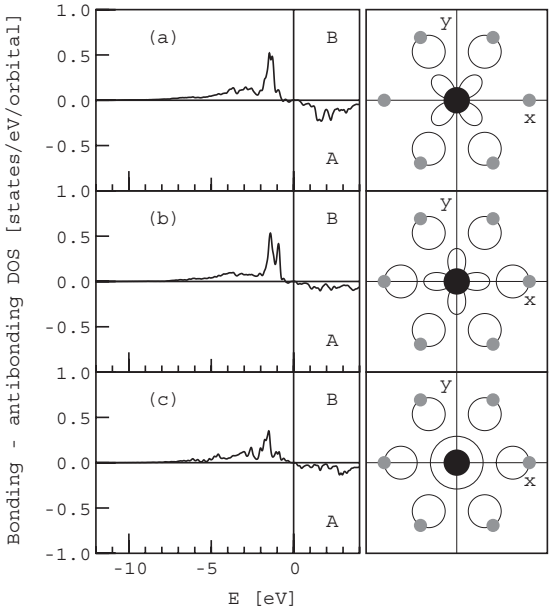

Figure 13. Differential COOP for bonding in the pseudohexagonal (001) plane of Al_2Fe with the C40 structure. The COOPs for individual Fe d orbitals with sp^2 hybridized orbitals on Al atoms are shown: (a) d_{xy}, (b) $d_{x^2-y^2}$ and (c) d_{z^2}. In the right panel the configurations of bonding orbitals are schematically displayed. Larger filled circles represent Fe, smaller grey circles Al atoms. The corresponding COOP is presented in the left panels. For each bonding configuration we see clear bonding–antibonding splitting of states. The COOP changes sign at the Fermi level. States below E_F have bonding character; states above E_F have antibonding character. We note that the d_{z^2} orbital has a significant bonding contribution in the (x, y) plane, despite its major orientation in the perpendicular direction.

exclude any orbital from a particular bonding configuration. Figure 14(b) shows the COOP for Fe–Al bonding. In the right panel the bonding configuration is schematically displayed; here the orientation of the bonding orbitals is not coaxial. The COOP in figure 14(b) again shows a clear bonding–antibonding splitting. From the charge density analysis we could conclude that there is no significant Fe–Fe or Al–Al bonding. This is demonstrated in figure 14(c), showing a possible bonding configuration and the corresponding COOP for two neighbouring Al atoms. A bond could be formed here by two overlapping p_z orbitals located on both Al atoms. However, the COOP in the left panel demonstrates that bonding between two Al atoms is negligible. We present this result for comparison with the C54 structure (see figure 19 below), where the situation is different.

From these results we can conclude that the clear bonding–antibonding splitting seen in the COOPs proves that the bonding in Al_2Fe in the C40 structure has covalent character.

7. Electronic structure of Al_2Fe in the C54 structure

The C54 structure exhibits the most pronounced semiconducting gap in the band structure of all crystal structures investigated. In this section we shall investigate this system in more detail.

7.1. Electronic density of states

The total and partial Al and Fe DOSs of Al_2Fe in the C54 structure have been presented in figure 2. Similarly as in the previous cases the partial Al DOS is dominated by s and p orbitals,

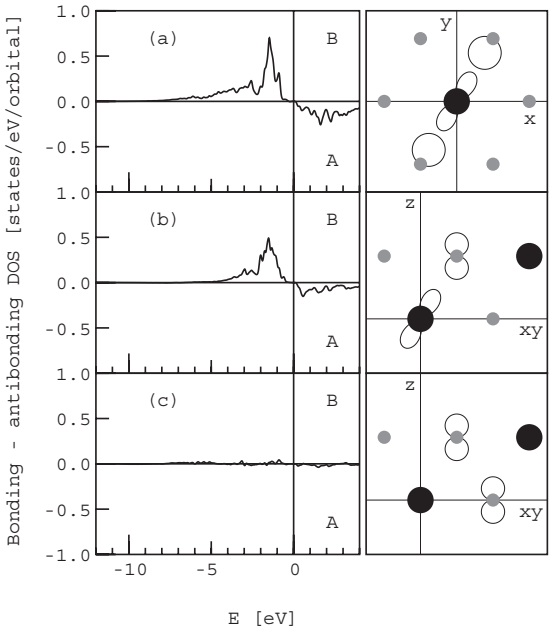

Figure 14. (a) COOP for bonding in the (001) plane of the C40 structure. A hybridized d^3 orbital on Fe interacts with two sp^2 hybridized orbitals on the Al atoms. (b) COOP for interplanar Fe–Al bonding. The d^4 hybridized orbital on the Fe atom is oriented towards the Al atom. From the Al side a p_z orbital oriented along the z-axis contributes to the bonding. (c) Bonding situation for two Al atoms in the (011) plane (cf figure 13).

but the contribution from d states is substantial at energies around E_F. The partial Fe DOS has around E_F almost uniquely d character; s states extend deeply below E_F. Figure 15 presents an orbital decomposition of the d DOS on the Fe atom. As the highest point-group symmetry D_{2h} is rather low, the splitting of the d band is not related to any symmetry splitting analogous to the well known e_g–t_{2g} splitting of d orbitals observed in a local field with O_h point-group symmetry. Each d orbital belongs to a different representation of the point group. From figure 15 one can see that all orbitals significantly participate in the bonding. The bonding is particularly strong for $d_{x^2-y^2}$ and d_{z^2} orbitals. For symmetry reasons bonding for d_{zx} is lowest.

7.2. Charge density distribution

Figure 16 shows a contour plot of the difference valence-charge distribution in the pseudohexagonal (001) plane. The positions of Fe atoms are marked by filled circles, positions of Al atoms are marked by open circles, regions of positive difference electron density in the (001) plane are shown with contour lines and in the blank space the difference density is negative. The difference charge distribution around the Fe atom has almost radial symmetry; only along the x-direction can weak maxima halfway between Fe and Al atoms be identified. Compared with the $C11_b$ or C40 structures the difference electron distribution is more evenly distributed. The Fe atom has ten aluminium neighbours; the remaining four Al neighbours can be found in the (011) and $(0\bar{1}1)$ planes. Figure 17 shows a contour plot of the difference valence-charge distribution in the (011) plane. As (011) and $(0\bar{1}1)$ planes are related by a pseudo-S_6 symmetry around the x-axis, the $(0\bar{1}1)$ plane exhibits a similar charge distribution. In the (011) plane in figure 17 we see regions of enhanced charge density halfway between the Fe atoms and Al neighbours, indicating covalent Fe–Al bonds. In addition we clearly see

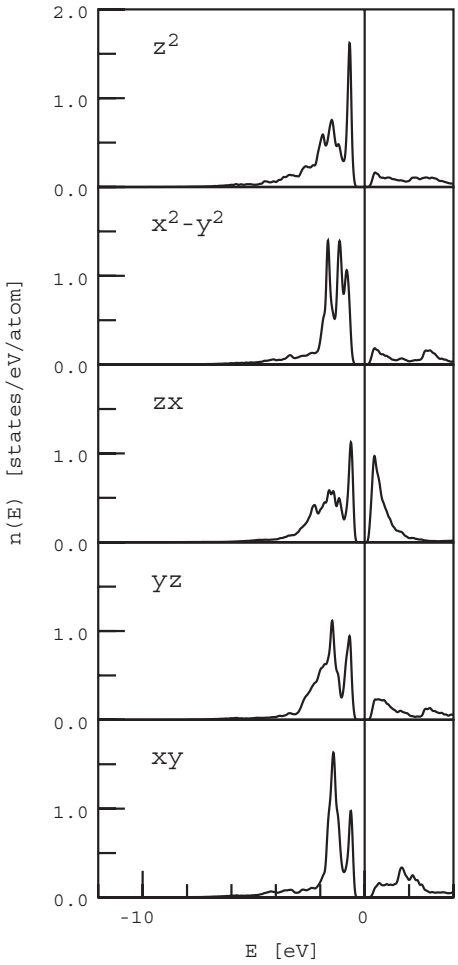

Figure 15. Orbital decomposition of the d DOS on the Fe atom in Al_2Fe with the orthorhombic C54 ($TiSi_2$) structure.

enhanced charge distribution between pairs of Al neighbours. It is also notable that there is no covalent bonding between Fe atoms.

In summary, there are several types of possibly covalent bond. In the pseudohexagonal (001) plane iron is covalently bonded to two Al atoms situated on both sides of Fe along the x-axis. These two bonds differ from the four bonds to the remaining four Al atoms in the plane. In the (011) plane we see two bonds along the x-axis with the same Al atoms as in the (001) plane, and two bonds with other Al atoms forming with the Fe atom in the centre an Al–Fe–Al bond angle of $\approx 147^\circ$. These two Al atoms with the two other atoms in the $(0\bar{1}1)$ plane form a distorted tetrahedral coordination around the Fe atom in the centre. The character of the bonds is investigated in the next section.

7.3. Hybridized orbitals and covalent bonding

The point-group symmetry of the Fe site in the C54 structure is rather low. Symmetry does not split any group of orbitals, neither does it exclude any orbital from the bonding. A clean

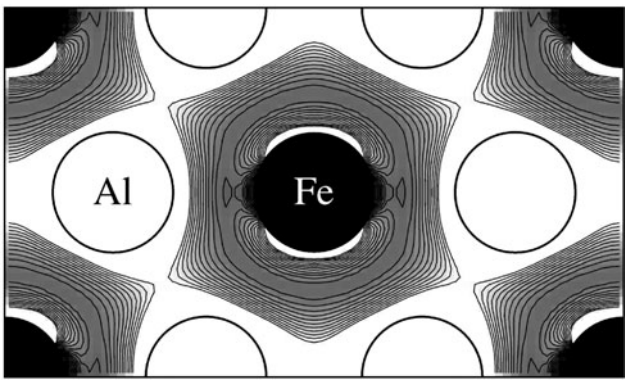

Figure 16. Charge-density distribution of Al_2Fe in the elementary cell of the C54 structure. The figure shows a contour plot of the difference valence-charge distribution in the (001) plane. The positions of Fe atoms are marked by filled circles; positions of Al atoms are marked by open circles. The contour plot represents regions of positive difference electron density; in the blank space the difference density is negative. A possible covalent bonding is indicated by enhanced charge distribution along connections between atoms. One can see a region of enhanced charge density halfway between the central Fe atom and six Al neighbours.

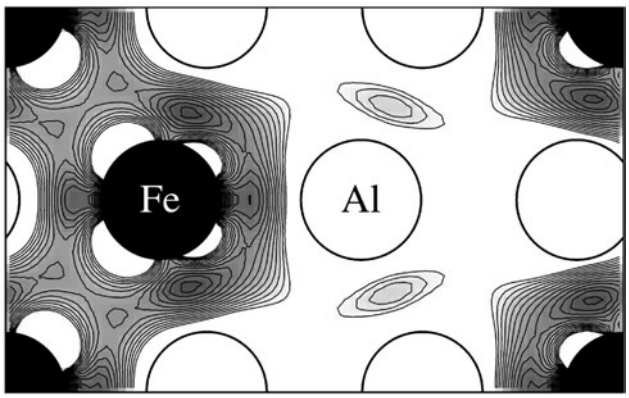

Figure 17. Contour plot of the difference valence-charge distribution for Al_2Fe (C54) in the (011) plane (cf figure 16). In this plane we see regions of enhanced charge density halfway between the Fe atoms and Al neighbours. In addition there are enhanced charge distributions between pairs of Al neighbours seen on the right side of the figure. There is no indication of bonding between Fe atoms.

gap in the band-structure hence indicates that if the bonding has covalent character and the gap originates from the bonding–antibonding splitting, than all orbitals must participate in the bonding. The molecular orbitals corresponding to the bonding and antibonding states include all orbitals in the system. On the other hand the C54 structure has only one inequivalent Al and one Fe site, which simplifies the picture of the bonding. The configuration of the Al orbitals participating in the bonding is quite simple. As each Al atom has in the pseudohexagonal (001) plane three Fe neighbours located at the vertices of a triangle, the symmetrized orbitals correspond to sp^2 hybrids formed by s, p_x and p_y orbitals. The remaining p_z orbital participates in bonding between neighbouring pseudohexagonal planes.

Participation of Fe d orbitals in the bonding is again more complex. It appears that all d orbitals participate in all bonds. Let us consider first bonding in the pseudohexagonal (001)

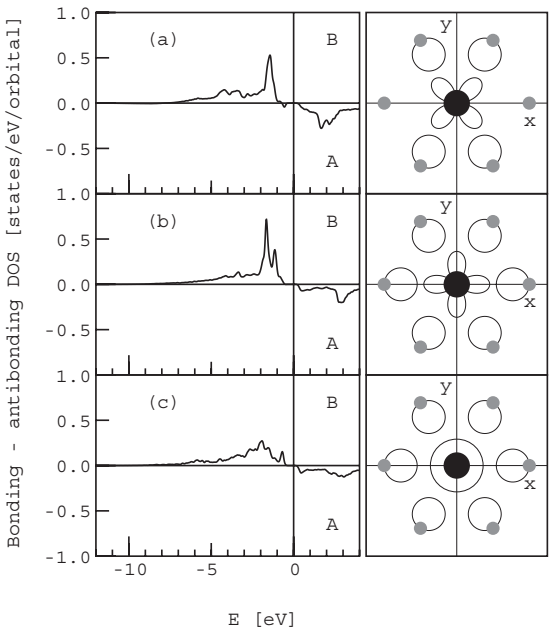

Figure 18. Differential COOP for bonding in Al_2Fe (C54) in the pseudohexagonal (001) plane. The COOPs for bonding of individual Fe d orbitals with sp^2 hybridized orbitals on Al atoms are presented: (a) d_{xy}, (b) $d_{x^2-y^2}$ and (c) d_{z^2} orbitals. In the right panel the configurations of bonding orbitals are schematically displayed. Larger filled circles represent Fe, smaller grey circles Al atoms. The corresponding COOP is presented in the left panels. For each bonding configuration we see clear bonding–antibonding splitting of states. The COOP changes sign at the Fermi level. States below E_F have bonding character; states above E_F have antibonding character. We note that the d_{z^2} orbital has significant bonding contribution in the (x, y) plane, although its major orientation is along the perpendicular direction.

plane. Figure 18 shows the COOP of several bonding configurations of individual d orbitals: part (a) shows the contribution of the d_{xy} orbital, (b) that of the $d_{x^2-y^2}$ orbital and (c) that of the d_{z^2} orbital to the bonding. For each orbital we see clear bonding–antibonding splitting of states. The COOP changes sign at the Fermi level: states below E_F have bonding character; states above the E_F have antibonding character. We note that even the d_{z^2} orbital makes a significant bonding contribution in the (x, y) plane despite its major orientation in the perpendicular direction. This illustrates the previous statement that each d orbital non-negligibly participates in all bonds. This also explains the relatively isotropic charge enhancement in the (001) plane around the Fe atom shown in figure 16. From the set of d orbitals we can also construct hybridized orbitals with a special orientation.

Figure 19(a) shows the COOP of a d^3 hybridized orbital which incorporates d_{xy}, $d_{x^2-y^2}$ and d_{z^2} orbitals on the Fe atom. Again we see clear bonding–antibonding splitting of the states. Interplanar bonding in the C54 structure is similar to that in the C40 structure. We present only the bonding configurations corresponding to the strong charge enhancement in the (011) plane shown in figure 17. Figure 19(b) shows the COOP for Fe–Al bonding. The d^5 hybridized orbital on the Fe atom oriented towards the Al atom includes all five d orbitals; from the Al side the p_z orbital oriented along the z-axis contributes to the bonding. Orientation of the bonding orbitals is here not coaxial. To explain this bonding situation we remark the following.

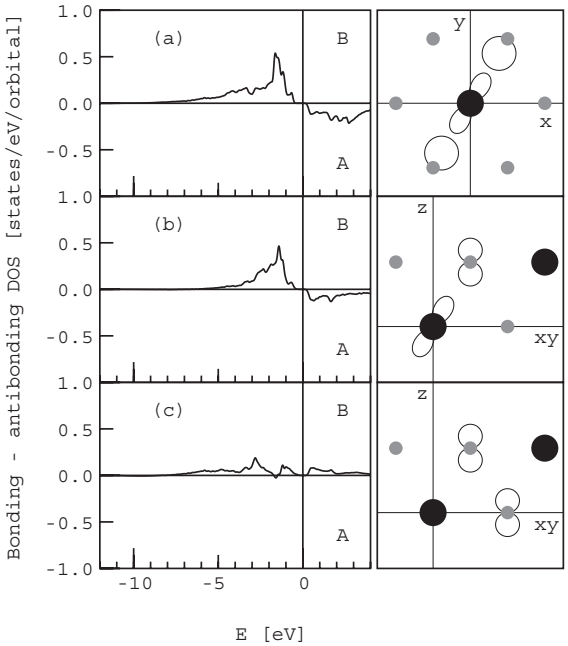

Figure 19. (a) COOP for bonding in the pseudohexagonal plane of Al_2Fe (C54). A hybridized d^5 orbital on the Fe atom interacts with two sp^2 hybridized orbitals on the Al atom. (b) COOP for interplanar Fe–Al bonding. The d^5 hybridized orbital (cf text) on the Fe atom is oriented towards the Al atom. From the Al side a p_z orbital oriented along the z-axis contributes to the bonding. (c) Bonding situation for two Al atoms in the (011) plane. The bonding configuration corresponds to the enhanced charge density due to Al–Al bonding seen in figure 17. Contrary to all previous results the COOP here is positive simultaneously below and above the Fermi level. This indicates that the Al–Al bond is here not fully saturated.

(i) Although in this picture p_z does not have the maximal overlap with the orbital centred at the Fe atom, we should keep in mind that d orbitals on Al atom that we have not considered so far hybridize with the p_z orbital and improve the overlap.

(ii) As we shall see below, the same p_z orbital also participates in the Al–Al bonding and overlaps with the p_z orbital from the other Al atom.

The COOP in figure 19(b) again shows a pronounced bonding–antibonding splitting.

Figure 19(c) shows the bonding configuration and the corresponding COOP for the Al–Al bonds seen in figure 17. The bond is formed by two overlapping p_z orbitals located on both Al atoms. Contrary to all previous results the COOP here is positive below and above the Fermi level. This also indicates covalent bonding; however, the Al–Al bond is not saturated and the bonding–antibonding splitting occurs at higher energies. The gap around E_F in the Al band thus requires little different explanation. The missing states here are absorbed in hybrid orbitals forming the Al–Fe covalent bonds.

The analysis of the COOP shows that in Al_2Fe with the C54 structure covalent bonds between Al and Fe atoms and also partially between Al and Al atoms are formed. There is no significant Fe–Fe bonding. The gap in the electronic band has the character of bonding–antibonding splitting of the electronic states.

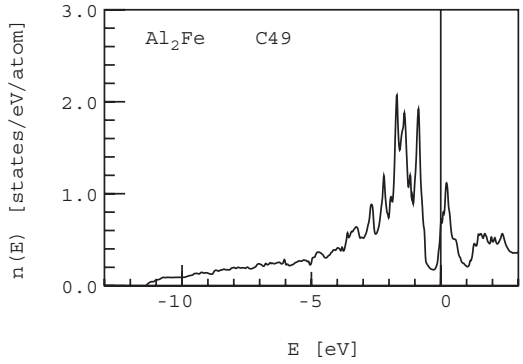

Figure 20. Total density of states of Al_2Fe in the C49 ($ZrSi_2$) crystal structure. The semiconducting gap in the band is missing here.

8. Electronic structure of Al_2Fe in the C49 structure

In the crystal structures investigated in previous sections a semiconducting gap at E_F is found in Al_2Fe and all homologous compounds. To better understand the mechanism of the bandgap formation we also present results for Al_2Fe in the C49 ($ZrSi_2$) structure, where no bandgap in the electronic structure is observed. The C49 structure also belongs to TM di-silicide structures. It is formed by a layered AB stacking of pseudohexagonal planes, but it differs from the family of C54, C40 and $C11_b$ structures in the chemical decoration of these planes. It can be derived from the $C11_b$ structure by interchanging two pairs of Al and Fe atoms in each layer. The interchange is demonstrated in figure 8. The interchange of site occupations breaks the pseudohexagonal symmetry in the (110) plane and has a dramatic effect on the resulting electronic structure.

The orthorhombic C49 structure, Pearson symbol oC12, belongs to the space group $Cmcm$ (No 63). There is one Wyckoff position (4c) with four independent sites (0, u, 0.25), (0, $\bar{u}$, 0.75), (0.5, 0.5 + u, 0.75) and (0.5, 0.5 − u, 0.25) for TM atoms and two 4c positions for Al atoms. The structure has thus three internal degrees of freedom—the parameters u for each Wyckoff position. The values of these parameters obtained by VASP are given in table 4. We note that in order to obtain the orientation of the elementary cell as shown in figure 8 one has to exchange y and z axes. The elementary cell contains 12 atoms. The number of nearest neighbours is the same as in the previously discussed structures. In comparison with the $C11_b$ structure the shape of the elementary cell is substantially elongated in the z-direction; the parameter $c/a = 4.029$ is greater by 42%. On the other hand the lattice parameter a is by 28% and b by 4% smaller than the corresponding dimension in the $C11_b$ structure.

8.1. Electronic density of states

Figure 20 shows the total DOS of Al_2Fe in the C49 structure—no semiconducting gap exists. However, a strong modulation of the DOS around the Fermi level and the existence of deep minima in the DOS at −0.3 and 1.0 eV indicate strong hybridization effects also in this structure. The total energy for this structural variant is 61 meV/atom higher than the total energy of Al_2Fe in the $C11_b$ structure and therefore it is only a hypothetical structure.

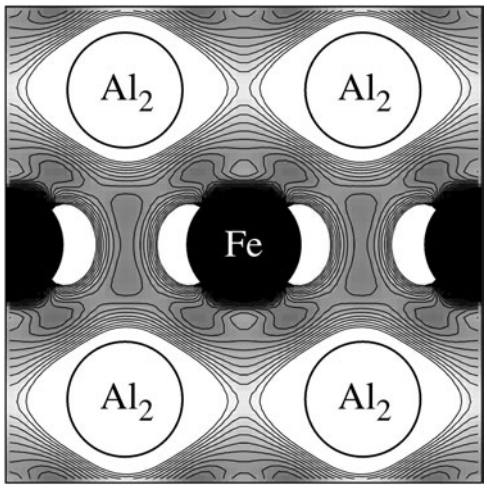

Figure 21. Charge-density distribution of Al_2Fe in the elementary cell of the C49 structure. The figure shows a contour plot of the difference valence-charge distribution in the (001) plane. A possible covalent bonding is indicated by enhanced charge distribution along connections between atoms. One can see a region of enhanced charge density halfway between the Fe atom and four Al_2 atoms located at the vertices of a rectangle.

Table 4. Equilibrium lattice parameters a, b/a and c/a, internal coordinates u, volume of the cell Ω and total energy E_{tot} of Al_2Fe with the C49 ($ZrSi_2$) structure.

a (Å)	b/a	c/a	$u(Al_1)$	$u(Al_2)$	u(Fe)	Ω (Å^3/atom)	E_{tot} (eV/atom)
3.066	4.029	1.326	0.7500	0.4334	0.0961	12.834	−5.5044

8.2. Charge density distribution

The interchange of occupation of two pairs of sites not only breaks the pseudohexagonal symmetry in the (110) plane but also the tetragonal space group symmetry is reduced to an orthorhombic one. The point group of the Fe site is C_{2v}. The pseudohexagonal (110) plane in the $C11_b$ structure now becomes the (100) plane and the former pseudohexagonal $(\bar{1}10)$, perpendicular to the (110) plane, now becomes the (010) plane. Aluminium sites are no longer equivalent and therefore we distinguish two sites, Al_1 and Al_2. Again, to study a possible covalent bonding we investigated the difference electron density. Figure 21 shows a contour plot of the difference valence-charge distribution in the (001) plane. The positions of Fe atoms are marked by filled circles. A possible covalent bonding is indicated by enhanced charge distribution along connections between atoms. We see regions of weakly enhanced charge density halfway between the Fe atom and the four Al_2 atoms arranged on the corners of a rectangle.

More interesting is the bonding in the (100) plane displayed in figure 22. This figure can be compared with figure 7 showing the corresponding plane in the $C11_b$ structure. The interchange of Fe and Al_2 atoms is indicated by arrows. Again one can recognize islands of weakly enhanced charge density between atoms. In this plane Fe atoms are weakly bonded to Al_1 atoms and some bonding charge is also recognizable between two Fe atoms. Much stronger bonds exist in the (010) plane (see figure 23). Note that the z-axis is here oriented horizontally. In this plane the pseudohexagonal arrangement of Al atoms around Fe atoms is still conserved, but the hexagon is strongly elongated along the z-axis. The picture of bonding

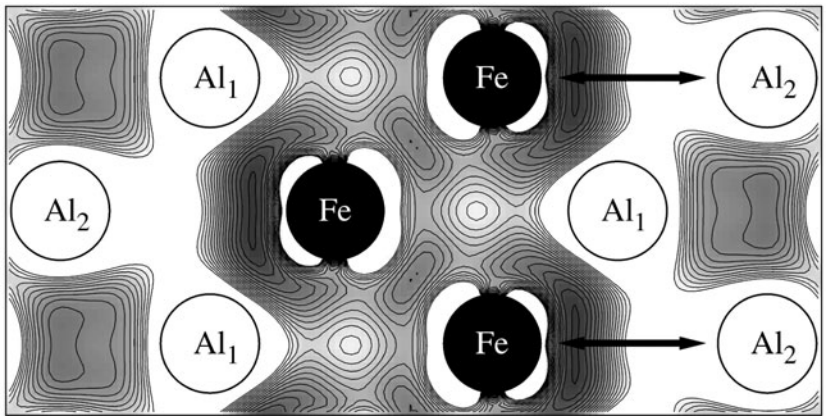

Figure 22. Contour plot of the difference valence-charge distribution in the pseudohexagonal (100) plane of Al_2Fe with the C49 structure. The horizontal direction corresponds to the z-axis. Arrows indicate atoms that are mutually interchanged in comparison with the $C11_b$ structure. (Compare with figures 8 and 7; see the text.)

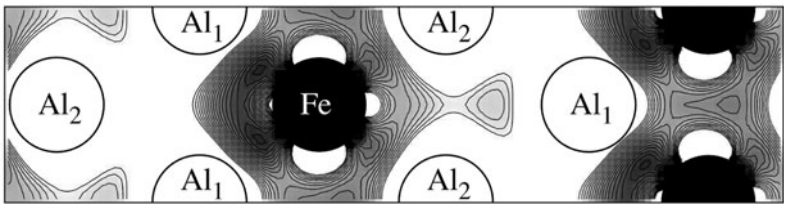

Figure 23. Contour plot of the difference valence-charge distribution in the pseudohexagonal (010) plane of Al_2Fe (C49). The horizontal direction corresponds to the z-axis. (Compare with figure 7; see the text.)

is here very similar to that in the (110) plane of the $C11_b$ structure (cf figure 7). An enhanced charge density is seen between Fe and the other four neighbouring Al atoms, but it is rather asymmetric, suggesting a stronger Fe–Al_2 than Fe–Al_1 bonding. The character of possible bonds is investigated in the next section.

8.3. Hybridized orbitals and covalent bonding

Figure 24 shows the differential crystal orbital overlap population, for (a) bonding of an Fe d^2 (d_{xy}, $d_{x^2-y^2}$) orbital with two p^2 (p_x, p_y) orbitals, (b) bonding of Fe d_{xy} orbitals with two Fe d_{xy} orbitals on a nearest-neighbour Fe atom and two sp^3 hybridized orbitals on Al_1 atoms and (c) bonding of a d^2 (d_{xz}, d_{z^2}) hybridized orbital on an Fe atom with an sp^3 hybridized orbital on Al_1 and an sp hybridized orbital on Al_2 atoms. In the right panels (a)–(c) the configurations of bonding orbitals that correspond to the charge density distributions presented in figures 21–23 are schematically displayed. The corresponding COOP is presented in the left panels. For bonding configurations (a) and (c) representing Fe–Al bonds we see a bonding–antibonding splitting of states similar to that in the $C11_b$ structure. A substantially different picture of bonding is seen in case (b), representing nearest-neighbour Fe–Fe bonds. While in cases (a) and (c) groups of bonding and antibonding states are separated by a narrow gap, in case (b) no such gap exists. Moreover, in case (b) significant antibonding states also exist below the Fermi level. From the comparison of the COOP shown in (b) with the total DOS in figure 20, it is clear that the states around the Fermi level are predominantly antibonding Fe states.

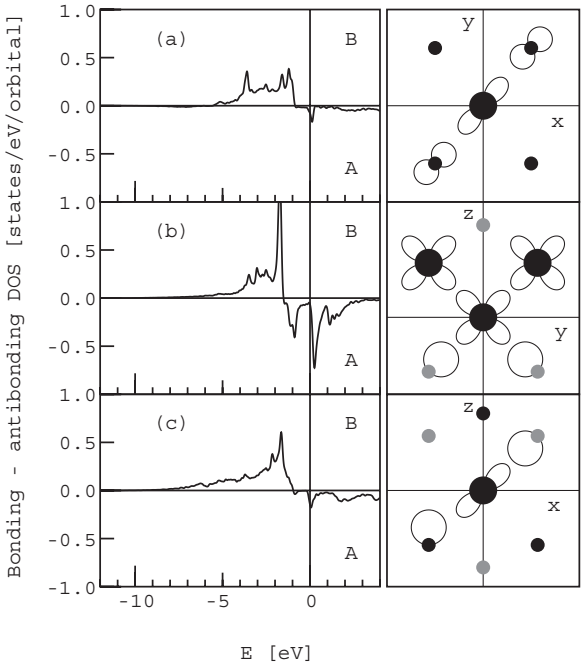

Figure 24. Differential COOP for C49-type Al_2Fe: (a) bonding of an Fe d^2 orbital with two Al p^2 orbitals, (b) bonding of Fe d_{xy} orbitals with two Fe d_{xy} orbitals on nearest-neighbour Fe and two sp^3 hybridized orbitals on Al_1 atoms and (c) bonding of a d^2 hybridized orbital on Fe atoms with an sp^3 hybridized orbital on Al_1 and an sp hybridized orbital on Al_2 atoms. Larger filled circles represent Fe, smaller grey circles Al_1 and black Al_2 atoms. In the right panels (a)–(c) the configurations of bonding orbitals that correspond to charge density distributions presented in figures 21–23 are schematically displayed. For bonding configurations (a) and (c) we see a bonding–antibonding splitting of states similar to the case of bonding in the $C11_b$ structure. While in the (a) and (c) cases groups of bonding and antibonding states are separated by a narrow gap, in the (b) case no such gap exists (cf text).

9. Discussion

The aim of our study is to explore the mechanism leading to the formation of a bandgap in the valence band of a rather wide class of TM di-aluminides and to the outstanding stability of this gap against replacement of the TM against elements from group VII to XI of the periodic table. For a critical band filling realized in the di-aluminides of the group VIII metals, the Fermi level falls into the gap and consequently Al_2Fe, Al_2Ru and Al_2Os with the $C11_b$, C40 and C54 structures (but not in the C49 structure) are predicted to be narrow-gap semiconductors.

From both the structural and electronic points of view, there is a strong similarity between these aluminides and the di-silicides of group IV–VI metals, which assume the same set of crystal structures and show semiconducting properties at the same critical electron-per-atom ratio ($e/A \approx 4.67$) as the di-aluminides [33–36]. However, the tendency to form a semiconducting gap seems to be even more pronounced for the aluminides than for the silicides: whereas in the series $CrSi_2$ (C40)–$MoSi_2$ ($C11_b$)–WSi_2 ($C11_b$) the width of the gap shrinks from 0.302 eV in $CrSi_2$ to 0.035 eV in $MoSi_2$ and is essentially zero in WSi_2, the di-aluminides show a tendency to widen the gap as the 3d metal is replaced by its 4d or 5d homologon. It is also remarkable that while in $CrSi_2$ the semiconducting gap exists only in the C40 and not in the C54 and $C11_b$ structures, the di-aluminides display a gap in all these

structural variants. Also, whereas all metals from groups IV–VI form a stable di-silicide, stable di-aluminides are found only for the group VIII metals—for other metals the di-aluminides are found to be unstable compared with a phase with a slightly different stoichiometry. Al_2Fe also is found to adopt a triclinic structure [15] with no symmetry and strange electronic as well as magnetic properties. This structure is highly disordered and the reasons for its stability are poorly understood. We shall return to triclinic Al_2Fe in a forthcoming publication.

Nonetheless, the present investigation is of interest in view of the observation of non-metallic behaviour in Al-based quasicrystals and related intermetallic compounds with a similar valence electron concentration. We hope to gain a general insight into the mechanism inducing non-metallic behaviour in compounds of metallic elements.

The earlier investigations of Mattheiss and others have already emphasized the important role of hybridization and dominant TM–Si bonding in determining the characteristic features of the band structure of these materials. However, gap formation requires more than a strong d–s, p hybridization: the bonding–antibonding splitting for all possible combination of hybrid orbitals must fall into the same energy range so that eventual gaps overlap. Evidently this requires that all atomic orbitals contribute to the bonding, and this in turn can be achieved only for a rather low site symmetry.

Our study confirms that the formation of strong TM–Al bonds gives by far the dominant contribution to the bonding in all three structures where a bandgap has been found. The situation is different in the C49 structure, where we have identified a strong TM–TM interaction that does not have the character of covalent bonding. The common structural element of the C54, C40 and $C11_b$ is the pseudohexagonal plane arranged in different stacking sequences. Within this plane, the point-group symmetry of the site occupied by TM atoms is rather low, leading to a participation of all d orbitals in the formation of TM–Al bonds. In the orthorhombic C54 structure all atomic d orbitals contribute to the interplanar TM–Al bonds formed by linear combinations of TM d^5-hybrid orbitals and Al p_z orbitals. The in-plane bonds also mix d_{xy}, $d_{x^2-y^2}$ and d_{z^2} states on the TM site with sp^2 hybrids on the Al sites. Evidently this favours the formation of a bonding–antibonding gap common to all bonds. The situation is similar in the C40 structure, where in-plane TM–Al bonds are formed by overlapping d^3 (d_{xy}, $d_{x^2-y^2}$, d_{z^2}) hybrids on TM with sp^2 hybrids on Al and where the bonding between planes is provided by TM d^4 (d_{xy}, d_{yz}, d_{zx}, d_{z^2}) hybrids overlapping with Al p_z orbitals. Only in the $C11_b$ structure have we found some TM–TM bonding via $d_{x^2-y^2}$ orbitals, but as the same orbital also contributes via the d^4 ($d_{x^2-y^2}$, d_{xy}, d_{yz}, d_{zx}) hybrid orbitals to the TM–Al bonds (overlap with sp^3 hybrids), the conditions for the formation of a common bandgap are also satisfied.

The revived interest in the semiconducting TM aluminides has been triggered partly by discovery of nearly insulating quasicrystalline phases—it does not seems to be a mere coincidence that the electron-per-atom ratio of 4.67 at which the di-aluminides and di-silicides become semiconducting is also very close to the valence-electron concentration of icosahedral AlPdRe which comes closest to semiconducting behaviour (in the electronic spectrum of this system we recently discovered [38, 39] a small gap very close to the Fermi level). In this context, the stability of the bandgap in the aluminides noted above could be important. Almost all known stable quasicrystals are ternary Al alloys with a high content of Al, and Al–TM_1–TM_2 alloys are all characterized by strong hybridization—even charge-density maxima characteristic for covalent bonding have been experimentally identified [37]. At present we are extending our studies in two directions: ternary Al_4–TM_1-TM_2 compounds with the crystal structures already considered in this work and icosahedral Al–TM_1–TM_2 quasicrystals. These studies will allow us to establish a strong link between the crystalline aluminides and the quasicrystals, which are all characterized by exotic transport properties.

Acknowledgments

This work has been supported by the Austrian Ministry for Education, Culture and Science through the Center for Computational Materials Science. MK also acknowledges support from the Grant Agency for Science in Slovakia (grant no 2/2038/22).

References

[1] Inoue A and Kimura H 2000 *Mater. Sci. Eng.* A **286** 1
[2] Inoue A, Kimura H, Sasamori K and Masumoto T 1996 *Mater. Trans. JIM* **37** 1287
[3] Stadnik Z M (ed) 1999 *Physical Properties of Quasicrystals (Springer Series in Solid-State Sciences)* (Berlin: Springer)
[4] Lue C S, Öner Y, Naugle D G and Ross J H 2001 *Phys. Rev.* B **63** 184405
[5] Weinert M and Watson R E 1998 *Phys. Rev.* B **58** 9732
[6] Watson R E, Weinert M and Alatalo M 1998 *Phys. Rev.* B **57** 12 134
[7] Watson R E and Weinert M 1998 *Phys. Rev.* B **58** 5981
[8] Watson R E, Weinert M and Alatalo M 2001 *Phys. Rev.* B **65** 014103
[9] Nguyen Manh D, Trambly de Laissardière G, Julien J P, Mayou D and Cyrot-Lackmann F 1992 *Solid State Commun.* **82** 329
[10] Öğüt S and Rabe K 1996 *Phys. Rev.* B **54** R8297
[11] Springborg M and Fischer R 1998 *J. Phys.: Condens. Matter* **10** 701
[12] Hoffmann R 1988 *Solids and Surfaces: a Chemist's View of Bonding in Extended Structures* (New York: VCH)
[13] Pearson 1972 *The Crystal Chemistry and Physics of Metals and Alloys* (New York: Wiley)
[14] Mattheiss L F 1991 *Phys. Rev.* B **43** 12 549
[15] Corby R N and Black P J 1973 *Acta Crystallogr.* B **29** 2669
[16] Kresse G and Furthmüller J 1996 *Comp. Mat. Sci.* **6** 15
Kresse G and Furthmüller J 1996 *Phys. Rev.* B **54** 11 160
[17] Kresse G and Joubert D 1999 *Phys. Rev.* B **59** 1758
[18] Vanderbilt D 1990 *Phys. Rev.* B **41** 7892
[19] Ceperley D M and Alder B J 1980 *Phys. Rev. Lett.* **45** 566
[20] Perdew J and Zunger A 1981 *Phys. Rev.* B **23** 5048
[21] Wang Y and Perdew J 1991 *Phys. Rev.* B **44** 13 298
[22] Perdew J, Chevary J A, Vosko S H, Jackson K A, Pederson M R, Singh D J and Fiolhais C 1992 *Phys. Rev.* B **46** 6671
[23] Andersen O K 1975 *Phys. Rev.* B **12** 3060
Skriver H L 1984 *The LMTO Method* (Berlin: Springer)
[24] Andersen O K, Jepsen O and Götzel D 1985 *Highlights of Condensed Matter Theory* ed F Fumi and M P Tosi (New York: North-Holland)
[25] Andersen O K, Jepsen D and Šob M 1987 *Electronic Band Structure and its Applications* ed M Youssouff (Berlin: Springer)
[26] Dronskowski R and Blöchel P E 1993 *J. Phys. Chem.* **97** 8617
[27] Bester G and Fähnle M 2001 *J. Phys.: Condens. Matter* **13** 11 541
[28] Sutton A P, Finnis M W, Pettifor D G and Ohta Y 1998 *J. Phys. C: Solid State Phys.* **21** 35
[29] Sutton A P 1993 *Electronic Structure of Materials* (Oxford: Oxford University Press)
[30] Krajčí M and Hafner J 2002 *J. Phys.: Condens. Matter* **14** 1865
[31] Krajčí M and Hafner J, at press
[32] Villars P 1997 *Pearson's Handbook* (Materials Park, OH: ASM International)
[33] Mattheiss L F 1991 *Phys. Rev.* B **43** 1863
[34] Mattheiss L F 1991 *Phys. Rev.* B **43** 12 549
[35] Mattheiss L F 1992 *Phys. Rev.* B **45** 3252
[36] McMahan A K, Klepeis J E, van Schilfgaarde M and Methfessel M 1994 *Phys. Rev.* B **50** 10 742
[37] Kirihara K, Nakata T, Takata M, Kubota Y, Nishibori E, Kimura K and Sakata M 2000 *Phys. Rev. Lett.* **85** 3468
[38] Krajčí M and Hafner J 1999 *Phys. Rev.* B **59** 8347
[39] Krajčí M and Hafner J 2001 *J. Phys.: Condens. Matter* **13** 3817